藥學碩士 學位論文

Structure-Based Discovery of *Mycobacterium tuberculosis* VapC30-Activating Stapled Peptides

Mycobacterium tuberculosis 유래 VapC30 구조기반 항생제 펩타이드에 관한 연구

2021年 2月

서울대학교 대학원
약학과 물리약학전공

한 상 우

Structure-Based Discovery of *Mycobacterium tuberculosis* VapC30-Activating Stapled Peptides

指導 敎授 李 奉 振

이 論文을 藥學碩士 學位論文으로 提出함
2020年 12月

서울大學校 大學院
藥學科 物理藥學專攻

韓 尙 佑

한상우의 藥學碩士 學位論文을 認准함

2020年 12月

委 員 長 _____ (印)
副委員長 _____ (印)
委 員 _____ (印)

Abstract

Structure-Based Discovery of *Mycobacterium tuberculosis* VapC30-Activating Stapled Peptides

HAN Sangwoo, physical pharmacy, the graduate school,
Seoul National University

Toxin-antitoxin (TA) systems have been considered essential factors for bacterial survival. During our drug development program aimed against tuberculosis (TB), we discovered certain peptides that mimic the binding of the VapBC30 complex, leading to the arrest of bacterial cell growth and eventually cell death. Herein, we optimized these candidate peptides based on a hydrocarbon stapling strategy and performed biological in vitro evaluations. The V30-SP-8 peptide successfully penetrated *Mycobacterium smegmatis* cell membranes and exerted bactericidal activity at a minimum inhibitory concentration that inhibited 50% of the isolates (MIC50) between 12.5 μM and 25.0 μM. With the aid of structural and biochemical information for the VapBC30 TA system from *M. tuberculosis*, we suggest potential antimicrobial agents that could provide a platform to establish a novel antibacterial strategy. Reflecting the limited number of therapeutic agents targeting TA systems, we believe that this study not only provides chemical tools for exploring the biological events relevant to TA systems but also opens a new gateway toward TB drug discovery.

Keyword : Toxin-antitoxin, tuberculosis, peptides, antimicrobial agents, novel antibacterial strategy
Student Number : 2019-26322

Table of Contents

Chapter 1. Introduction

Bacterial toxin–antitoxin (TA) systems play essential roles in cell survival as coupled regulators. Typically, toxins serve as negative regulators and are involved in various functions, such as RNA cleavage, acetylation, phosphorylation, and ATP synthesis inhibition *(1)*. Throughout these control events, toxins lead to growth arrest and eventual death of bacterial cells. In contrast to toxins, antitoxins act as positive regulators in cell survival through the neutralization of RNase activity by binding to their cognate toxins at either the protein or gene level. Under various stress conditions such as a shortage of nutrients or treatment with antibiotics, bacteria take advantage of mechanisms associated with a balance between toxin and antitoxin expression levels to maintain homeostasis. Since TA systems are strongly related to bacterial survival, TA systems are recognized as promising antibacterial targets for the development of new antimicrobial agents *(2, 3)*.

In *Mycobacterium tuberculosis (M. tuberculosis)*, there are abundant TA systems in the whole genome. Surprisingly, proteins belonging to the TA system account for more than 5% of all proteins in the H37Rv strain. Since the treatment of *M. tuberculosis* infections still requires combination therapy for a long period of time, especially in the cases of multidrug–resistant tuberculosis (MDR–TB) and extensively drug–resistant tuberculosis (XDR–TB), novel antimicrobial agents with a new mode of action, distinct from that of classic antibiotics, are needed. As cumulative studies indicate that TA systems are probably relevant to the infection and pathogenicity of bacteria *(1)*, their functional and regulative roles in bacterial survival have been widely discussed over the last decade *(4, 5)*. Specifically, structure–function relationship studies of TA systems from *M. tuberculosis* have provided information for protein–protein interactions (PPIs) between toxins and antitoxins, which can be a promising therapeutic target in the development of

novel antimicrobial agents *(6)*. In particular, the fact that TA systems, though frequently prevalent in bacterial pathogens, are not present in eukaryotic cells makes them even more attractive targets *(1, 7)*. In this strategy, we envisioned disturbing the interaction between a toxin and an antitoxin by small molecules, which would induce the RNase activity of toxin proteins by taking antitoxin proteins apart *(1, 7)*.

We previously reported that three helical peptide segments, designed by utilizing the crystal structure of the *M. tuberculosis* VapBC30 complex (*Rv0623–Rv0624*, PDB ID: 4XGQ), mimic the binding interface between VapC30 and VapB30 and exhibit inhibitory activity toward the corresponding TA complex *in vitro (8)*. In general, however, linear peptides have drawbacks, including poor cell permeability and proteolytic stability. In addition, high conformational flexibility contributes to a low binding affinity to target proteins, resulting in poor bioactivity. To circumvent such issues, a peptide stapling strategy devised by Verdine and coworkers was adopted *(9)*. In this work, we suggest that the potential toxin activator V30-SP-8 targets the VapBC30 TA system in *M. tuberculosis*. Moreover, cell growth was inhibited when the VapBC30 system was transferred to *M. smegmatis* and knocked out of VapB30 *(10)*. Considering the role of TA systems in *M. tuberculosis*, this study might provide chemical tools for exploring biological events relevant to the TA systems of *M. tuberculosis*

Chapter 2. Result and Discussion

2.1. Alanine Scanning of Linear Peptides and Design of Stapled Peptides

As previously reported by our group, the helical fragments at the binding interfaces of either VapC30 or VapB30 serve as inhibitors of the corresponding TA PPI (8). To determine the contribution of each residue to the inhibitory activity and to elucidate the suitable position of nonnatural amino acids for peptide stapling, alanine scanning was performed (Figure 1a). Each peptide with an alanine substitution was added to the VapBC30 complex to evaluate if it leads to the exposure of the RNase activity of VapC30 through an in vitro RNase assay. For the VapB30 α152–59 peptide, none of the mutant peptides showed a considerably noticeable change in the inhibitory activity (<10% drop in comparison with that of the wild-type peptide). Thus, we chose the positions of the olefin-bearing residues (Figure 1b) according to the following standards: i) less than 5% change in the inhibitory activity when alanine was substituted and ii) two locations at i and i+3, 4 or 7 were chosen to align these residues in the same helical face. In the case of double-stapled (stitched) peptides, the B5 residue was incorporated in the middle of two nonnatural amino acids at i and i+7 (Figure 1c). For the other two linear peptides (VapC30 α214–30 and VapC30 α448–56), some mutants (E6A, R7A, F8A, E9A, V12A, and E13A for the former; R1A, E4A, G7A, R8A, and E9 for the latter) lost activities of more than 10% toward the TA complex compared to the corresponding original peptides (Figure 1a). Based on these results, we determined the suitable positions for stapling residues to generate proper synthetic targets (Figure 1d). For some VapC30 α214–30 derivatives, those without any contribution to the inhibitory activity were truncated (entries 6 and 11, Figure 1d)

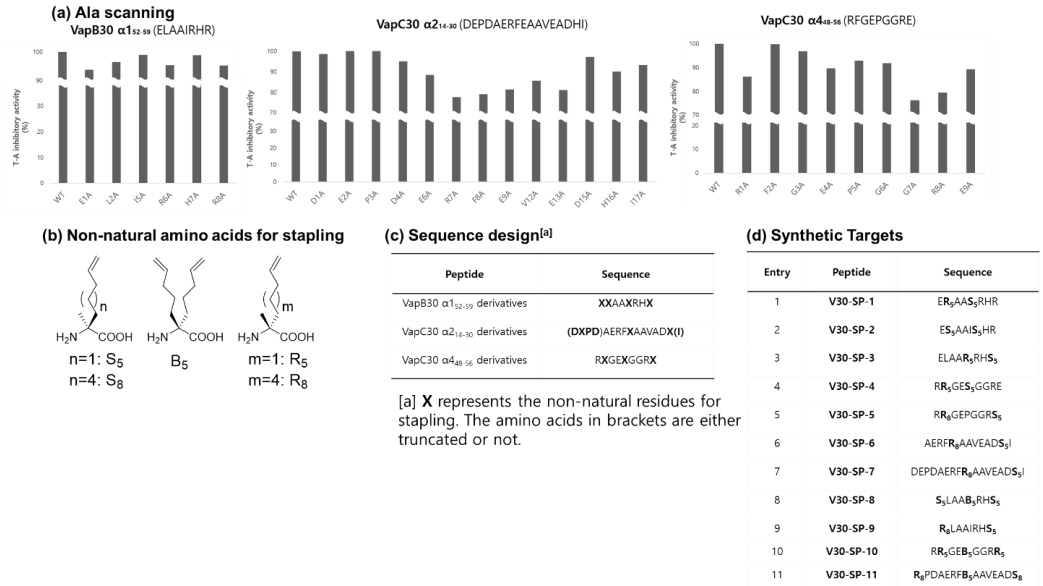

Figure 1 Design of stapled peptides based on alanine scanning. a) Alanine scanning results of three VapBC30-originating linear peptides (VapB30 α152-59, VapC30 α214-30, and VapC30 α448-56). The activity was normalized to that of the original peptide. b) Olefin-bearing nonnatural amino acids used for peptide stapling. c) Determination of the positions of stapling residues. d) Synthetic targets.

2.2. *In Vitro* RNase Assay Against Stapled Peptides

Based on the alanine scanning results, a total of 11 stapled peptides were prepared throughout solid-phase peptide synthesis with purities above 95% (Figures 1d and S1, Table S1) and further characterized by high-resolution mass spectroscopy. To examine their ability to disrupt the interaction within the VapBC30 complex, we performed an *in vitro* RNase assay. In this assay, the inhibitor peptides would release the VapC30 toxin protein from the VapB30

antitoxin protein, leading to the recovery of VapC30 RNase activity. Subsequently, the substrate RNA, which serves as a linker between a fluorophore and a quencher, is cleaved, thereby increasing the fluorescence intensity in proportion to the number of free VapC30 toxin proteins (Figure 2a).

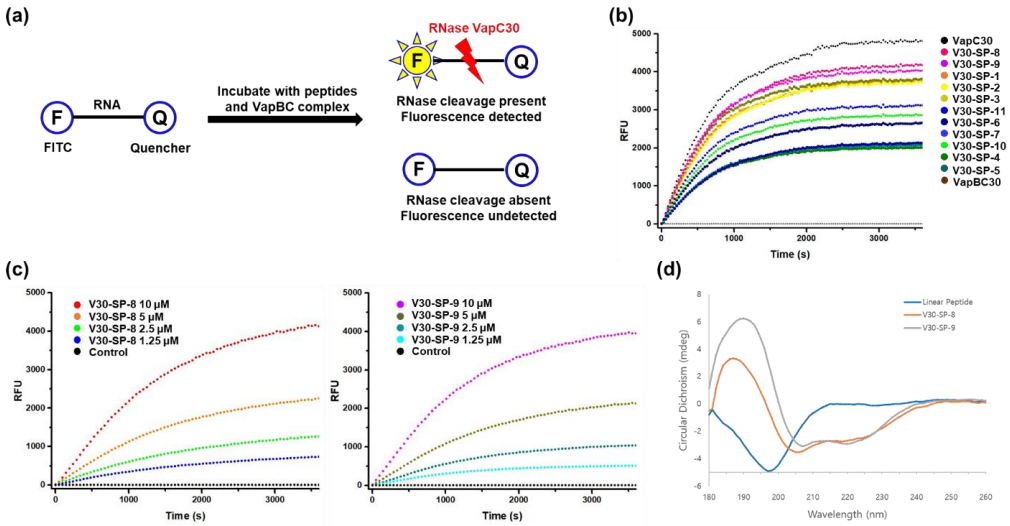

Figure 2 *In vitro* assay data for stapled peptides. a) Schematic diagram of the *in vitro* ribonuclease activity assay. b) *In vitro* ribonuclease activity assays of synthetic stapled peptides. c) Concentration-dependent ribonuclease activities of **V30-SP-8** (left) and **V30-SP-9** (right). d) CD spectra of **V30-SP-8** and **V30-SP-9**.

In the initial assessment, the comparison among the stapled peptides was conducted by treating the same amount of compounds (10 μM) with the mixture of TA complex and substrate RNA. As a result, the five stapled peptides modified upon the addition of VapB30 $\alpha 1_{52-59}$ peptide were found to be superior to the other stapled peptides in terms of the disruption activity (entries 1-3, 8, and 9, Figure 1d). Among them, **V30-SP-8** and **V30-SP-9** were shown to be the most effective peptides (Figure 2b). These peptides mimic the toxin-binding region of VapB30 and were designed to bind to the nonactive site of VapC30. Therefore, **V30-**

SP-8 and V30-SP-9 compete with VapB30 for binding to VapC30, consequently exposing the active site of VapC30 and leading to the digestion of the bacterial RNA. In this way, our stapled peptides could act as antibacterial agents against VapBC30-expressing pathogens such as *M. tuberculosis*. The concentration dependence of these peptides was also confirmed (Figure 2c). A previous study of VapBC30 *(8)* reported that 10 μM of linear peptide presents sufficient complex-disrupting activity. Based on these results, we determined the concentration of V30-SP-8 and V30-SP-9 for further studies and showed that they exhibit activities at less than 10 μM. V30-SP-8 and V30-SP-9 were modified from the same linear peptide but are different in the stapling linker used in their synthesis. Cell inhibitory properties have a complexed effect based on their peptide helical nature and cell permeability, which contribute to the dissociation of VapC from VapBC30. Therefore, although similar *in vitro* RNase activities are observed, the two stapled peptides may present differences in their helicity and corresponding cell membrane permeabilities.

2.3. CD Spectrometry of Linear Peptides and Stapled Peptides

The helical propensities of two stapled peptides, V30-SP-8 and V30-SP-9, and their linear counterparts were analyzed via circular dichroism (CD) spectrometry. While a strong negative peak at approximately 195 nm appeared for the linear peptide, which indicates a typical pattern of random coil, the stapled peptides showed two negative peaks at 208 and 222 nm, indicating a helical structure in aqueous media (Figure 2d). Surprisingly, in contrast to our expectation that the stitched peptide, V30-SP-8, would be more helical than the mono-stapled peptide, V30-SP-9, the

mono-stapling strategy was more effective in inducing helicity (helicity: 26.1% for **V30-SP-8** and 33.8% for **V30-SP-9**). This result might indicate that there is further room for the structural optimization of the stitched peptide. In the case of the linear peptide, 2,2,2-trifluoroethanol (TFE) was added to the solvent to induce the helical structure. Even though the solvent was completely exchanged with TFE, it failed to increase the helicity to the same level as that of the stapled peptides in the TFE-free solvent (Figure S2). Accordingly, this result features the effectiveness of our peptide stapling strategy.

2.4. Evaluation of Cell Permeability

To investigate whether the stapled and linear peptides penetrate *M. smegmatis* cell membranes, confocal microscopy studies using fluorescein isothiocyanate (FITC)-labeled **V30-SP-8** and **V30-SP-9** and the linear form of these two stapled peptides were performed in VapBC30-harboring *M. smegmatis* (Figure 3a-d). In the case of the linear peptide, a fluorescence signal was rarely observed inside cells, implying its poor ability to pass through the bacterial membrane (Figure 3b). According to the CD spectroscopic analysis, the linear peptide does not form an α-helical structure in aqueous media, attributing to the low cell permeability. In contrast, **V30-SP-8-FITC** and **V30-SP-9-FITC** were taken up by *M. smegmatis* (Figure 3c and d), which again correlates with the helical propensities. The cellular uptake of stapled peptides was approximately 2-fold higher than the linear peptide cellular uptake (Figure S3). Thus, the stapling technology successfully enhanced the cell membrane penetration and localization of peptides in the cell. More images are available in Figure S4.

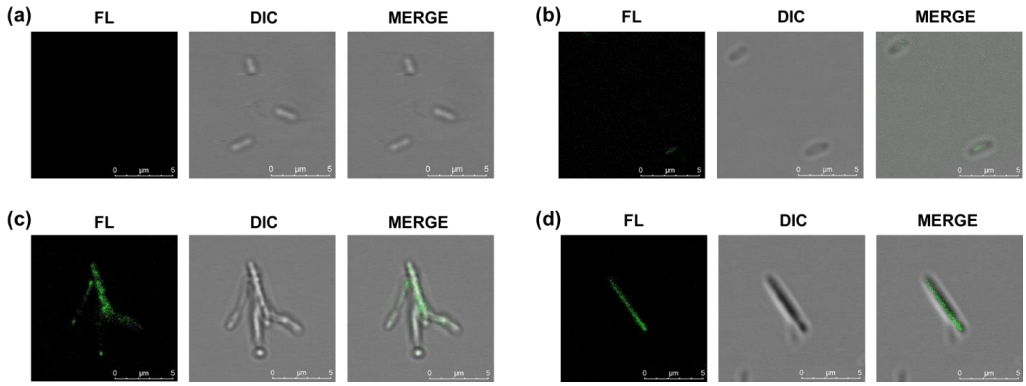

Figure 3 Confocal laser scanning microscopy images of *M. smegmatis* treated with FITC-labeled peptides (10 μM) (left), bright-field images of *M. smegmatis* (middle) and merged images (right) are presented. a) Blank control. b) Linear peptide. c) **V30-SP-8**. d) **V30-SP-9**

2.5. Antibacterial Activity of V30-SP-8 and V30-SP-9

In our previous study, it was observed that the expression of VapC30 alone without VapB30 led to bacterial cell death *(8)*. Based on the results, we hypothesized that a chemical tool that dissociates VapC30 from VapB30 would exhibit antibacterial activity. To support this hypothesis, *M. smegmatis* mc^2155 cells were treated with stapled peptides and the linear counterpart. Our antimicrobial activity test revealed that cell growth was inhibited at 6.25 μM **V30-SP-8** and **V30-SP-9**. Because this test was performed by the 2-fold dilution method as described in the methods section, inhibition at the concentrations of 6.25 μM, 12.5 μM, 25 μM and 50 μM (more than 6.25 μM) was further evaluated in the next flow cytometry study. Then, the effect of the addition of **V30-SP-8** and **V30-SP-9** on *M. smegmatis* mc^2155 cells was

tested by flow cytometry analysis of cells labeled with LIVE/DEAD BacLight stains (Figure 4a). *M. smegmatis* mc^2155 cells treated with 70% isopropyl alcohol and DMSO had 96% and 25% dead cells, respectively, which are permeable to propidium iodide (PI). When *M. smegmatis* mc^2155 cells were treated with the stapled peptides, the proportion of PI-permeable cells increased with the concentration of the peptides, indicating the bactericidal activity of the structure-based designed peptide. Because the successful internalization of **V30-SP-8** was demonstrated by confocal images (Figure 3b and c), the results indicate that the bactericidal effects were indeed exerted inside the bacterial cells. When the bactericidal activities of **V30-SP-8** and **V30-SP-9** were normalized to that of 70% isopropyl alcohol and DMSO as 100% and 0%, respectively, the minimum inhibitory concentration that inhibited 50% of the isolates (MIC_{50}) value of **V30-SP-8** was between 12.5 μM and 25.0 μM (Figure 4b), which showed a similar potency to vancomycin (MIC_{50} = 20 μM against *M. smegmatis*) with respect to antibacterial activity according to previous studies *(11, 12)*. In our opinion, because helicity is one of the important factors that affects cell permeability *(9)*, the helicity differences among the tested peptides might explain the lower effect of the linear peptide at 50 μM compared with that of the stapled peptide at 6.25 μM. These data show significant potential for **V30-SP-8** for applications in the field of antibacterial drug discovery.

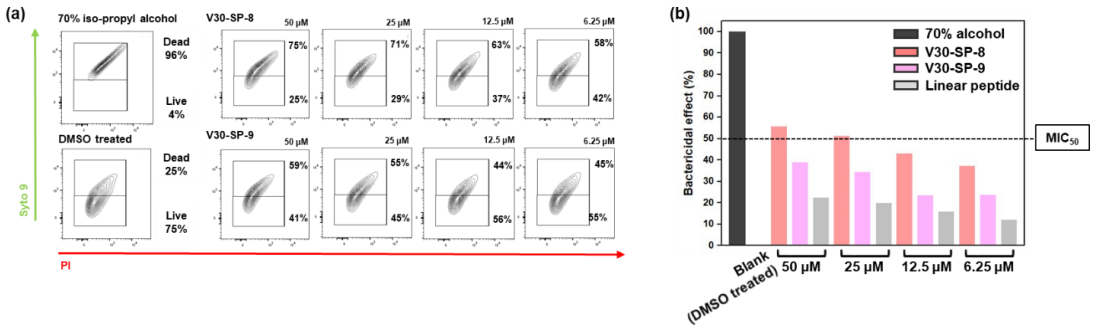

Figure 4 Antibacterial activities of **V30-SP-8** and **V30-SP-9**. a) *M. smegmatis* was treated with various concentrations of **V30-SP-8** and **V30-SP-9**. The cells were labeled with LIVE/DEAD BacLight stains (Syto 9; propidium iodide (PI)) and analyzed by fluorescence-activated cell sorting (FACS). The bactericidal activity of 70% isopropyl alcohol represents a positive control. Live cell/dead cell areas were established using this control. b) Bar graph for FACS data. The histogram is representative of three sets of independent experiments.

Chapter 3. Conclusions

In this work, we developed a novel stapled peptide, **V30-SP-8**, which targets the VapBC30 TA protein complex. The design of peptide sequences by alanine scanning and subsequent screening throughout the *in vitro* RNase assay showed **V30-SP-8** and **V30-SP-9** as peptide hits. CD spectroscopy analysis and confocal laser scanning microscopy showed the correlation between α-helicity and cell permeability, thereby proving the effectiveness of our approach. Treatment of the stapled peptides with *M. smegmatis* resulted in **V30-SP-8** exhibiting antimicrobial activity with an MIC_{50} between 12.5 μM and 25.0 μM, which was comparable to that of vancomycin. Taken together, these results indicate that our novel stapled peptide, **V30-SP-8**, exerts great bactericidal activity by disturbing the interaction within the VapBC30 protein complex. The mode of action of **V30-SP-8** is distinguished from the typical antimicrobial agents that generally block DNA, RNA, protein, or cell wall synthesis. This feature infers that **V30-SP-8** could presumably be a promising chemical source to address drug resistance. Given the abundance of TA systems, including VapBC30 in *M. tuberculosis*, we expect that our studies could contribute to the elucidation of unraveled biological events relevant to TA systems.

Chapter 4. Experimental methods

4.1. Protein Preparation

The TA complex protein VapBC30 as well as the VapC30 protein alone were overexpressed in E. coli cells and purified using the same procedures as in a previous paper (8).

4.2. Peptide Synthesis

Peptide synthesis was performed as previously reported using Fmoc-protected amino acids and rink amide MBHA resin *(13, 14)*. Detailed synthetic procedures as well as spectroscopic results can be found in the Supporting Information (Figure S1 and Table S1).

4.3. *In Vitro* Ribonuclease Assay

The ribonuclease activity of VapC30 released from VapBC30 by peptides was confirmed using an RNase Alert Kit (IDT, Coralville, IA, USA). In this assay, a fluorophore is covalently attached to one end of a synthetic RNA strand and quenched by a quencher group at the other end of the synthetic RNA. If synthetic RNA containing a fluorophore-quencher pair interacts with ribonuclease, the synthetic RNA is digested, and fluorescence is detected. The released fluorophore emits fluorescence at 520 nm upon excitation at 490 nm. The resulting fluorescence (relative fluorescence units, RFUs) was observed on a SpectraMax Gemini XPS Microplate Reader (Molecular Devices, San Jose, CA, USA). Various concentrations of peptides (1.25, 2.5, 5, and 10 μM), 10 μM VapC30 toxin and 10 μM VapBC30 complex were used.

4.4. CD Spectroscopy

CD measurements were performed using a Chirascan-Plus spectropolarimeter (Applied Photophysics, Leatherhead, UK) at 20° C in a cell with a 1-mm light path. The peptide samples were prepared with concentrations of 50 μM in a mixture of water and acetonitrile (9:1, *v/v*). TFE was serially added (1, 10, 20, 50, 100%) to the solvent for the analysis of the linear peptide only. CD scans were taken from 180 nm to 260 nm with a 1 nm bandwidth and a scan speed of 100 nm/min. Three scans were averaged, and the solvent background was subtracted from the averaged scans. The helicity of each peptide was calculated by CDNN software *(15)*.

4.5. Cloning and Expression in *M. smegmatis*

The genes encoding *M. tuberculosis* (strain H37Rv) VapB30 (*rv0623*) and VapC30 (*rv0624*) were amplified using primers Rv0623-BHI_F, Rv0623-Hid_rN, Rv0624-Ndel_F, and Rv0624-ERV-R (Table S2) and cloned into the expression vector pYUBDuet (Addgene, Watertown, MA, USA) to enable the production of VapB30 with an N-terminal hexa-histidine tag and VapC30. The vector harboring *rv0623* and *rv0624* was transformed into *E. coli* Top10 competent cells (Thermo Fisher Scientific, Waltham, MA, USA). The plasmid extracted from transformed Top10 cells was electroporated into *M. smegmatis* mc^2155. Preparation of *M. smegmatis* competent cells and electroporation were conducted following reported protocols (Bio-Rad, Hercules, CA, USA, www.Bio-Rad.com). *M. smegmatis* mc^2155 strains harboring *rv0623* and *rv0624* were grown in Middlebrook 7H9 liquid culture medium supplemented with 10% albumin-dextrose-saline (ADS), 0.5% glycerol and 0.1% Tween 80 at 37° C and 100 rpm. Hygromycin (Hyg) 50 μg/ml was used in the culture of *M. smegmatis*. As the OD_{600} of the culture reached 0.5, expression was induced by the addition of 0.5 mM isopropyl 1-thio-D-galactopyranoside, and the culture was grown at 37° C for 24 hours.

4.6. Confocal Microscopy

Confocal microscopy (Leica Microsystems, Wetzlar, Germany) was used to assess the permeability of peptides into *M. smegmatis* using FITC-labeled peptides. Cultures of *M. smegmatis* grown in complete 7H9 medium to midlogarithmic phase (OD_{600} 0.3-0.5) were diluted in Mueller-Hinton broth (BD Bioscience) to a 5-fold dilution. Diluted cell suspensions aliquoted in Eppendorf tubes were treated with antimicrobial peptide agents at 10 μM. After 1 hour of incubation at 37° C and 100 rpm, the cell suspensions were washed with phosphate buffered saline (PBS). Images were acquired on a TCS8 confocal microscope (Leica Microsystems, Wetzlar, Germany) with a 63x oil immersion objective.

4.7. Antimicrobial Activity Test (MIC Test)

The minimum inhibitory concentration (MIC) of several antimicrobial peptide agents for VapBC30 harboring *M. smegmatis* was determined with the twofold serial dilution method in 7H9 medium. Log-phase cultures of *M. smegmatis* were diluted to an OD_{600} value of 0.01. Two hundred microliters of diluted cultures were inoculated in a 96-well plate (polystyrene rounded square well, SPL, South Korea), and 100 μL of peptide solutions with a concentration from 100 μM to 3.125 μM were added into each well. Visible growth was scored after 1 day of incubation at 37° C. The wells containing bacterial pellets were denoted as the positive wells, whereas the wells containing clear broth were denoted as the negative wells. The MIC was defined as the lowest peptide concentration that completely inhibited bacterial growth. Each test was conducted in duplicate.

4.8. Flow Cytometry

Flow cytometry was used to assess both the permeability and viability of peptides to *M. smegmatis*. The preparation of samples for permeability assessment followed the same protocol as the preparation of samples for confocal images. For viability analysis, *M. smegmatis* harboring VapBC30 was grown in complete 7H9 medium to the midlogarithmic phase (OD_{600} 0.3−0.5) and treated with antimicrobial peptide agents at 10 μM. After 24 hours of incubation at 37° C and 100 rpm, the cells were stained with a LIVE/DEAD BacLight Bacterial Viability Kit (Invitrogen) containing PI−phycoerythrin (PE) and Syto 9−FITC. Both flow cytometry analyses were performed on a FACSLyric (BD Bioscience, US), and data were analyzed using FlowJo software (TreeStar).

Chapter 5. Supporting Information

5.1. Peptide synthesis

Peptide synthesis was conducted using a slightly modified procedure *(1, 2)*. The peptides were prepared using Fmoc chemistry on Rink Amide MBHA Resin (BeadTech) with a loading capacity of 0.41 mmol/g. All syntheses were conducted on an 82 μ mol scale. The dry resin was swelled with *N*,*N*−dimethylformamide (DMF) for 2 h before use. The Fmoc protecting group was removed by treatment with 20% piperidine in DMF (2 × 10 min). After Fmoc deprotection, the resin was washed with DMF (×3), MeOH (×3), dichloromethane (DCM, ×3), and *N*−methylpyrrolidone (NMP, ×3). Both natural and nonnatural amino acids were coupled for 2 h using 4 equivalents (eq) of 1−cyano−2−ethoxy−2−oxoethylidenaminooxy)dimethylamino−morpholino−carbenium hexa fluorophosphate (COMU) as an activating agent, 4 eq of Fmoc−protected amino acid, and 8 eq of diisopropylethylamine (DIPEA) in NMP. After thoroughly washing with DMF (×9), the completeness of the coupling reaction was confirmed by the Kaiser test.

5.2. Metathesis and purification

Ring−closing metathesis of resin−bound *N*−Fmoc, side−chain−protected peptides was performed using 20 mol % Grubbs catalyst in 1,2−dichloroethane (DCE) for 2 h at room temperature under an Ar atmosphere. After washing with DCM (×2), MeOH (×2), and DCM (×2), the reaction was repeated an additional 2 times. The reaction was monitored using an Agilent HP 1260 system (Agilent Technologies, Santa Clara, CA) after the cleavage of the peptides from a resin aliquot. After Fmoc removal, the *N*−terminus modification of the peptides with either an acetyl group or fluorescein isothiocyanate (FITC) was performed according to the

following conditions: i) acetylation: acetic anhydride (30 eq) and diisopropylethylamine (60 eq) in NMP for 45 min at room temperature; ii) FITC labeling: FITC (1.5 eq) in pyridine/DMF/DCM (*v/v/v* = 12/7/5) overnight at room temperature. The resin was washed with DMF (×3), MeOH (×3), and DCM (×3) and dried under vacuum overnight. The peptide was deprotected and cleaved from the resin by treatment with a mixture of trifluoroacetic acid/triisopropylsilane/water (*v/v/v* = 95/2.5/2.5) for 2 h. Then, the volatile components were removed under reduced pressure. The crude mixture was dissolved in a 1:1 mixture of acetonitrile and water and filtered through a 0.45 μm syringe filter. The desired product was purified by reverse-phase high-performance liquid chromatography (HPLC) using a Zorbax C18 column (Agilent, 5 μm, 80 Å, 21.2 × 150 mm) and characterized by liquid chromatography-mass spectrometry (LC-MS) analysis as well as an ultra-high resolution electrospray-ionization quadrupole time-of-flight (ESI Q-TOF) mass spectrometer (Bruker, US) at the Organic Chemistry Research Center of Sogang University (Republic of Korea).

REFERENCES

1. Hilinski, G. J., Kim, Y.-W., Hong, J., Kutchukian, P. S., Crenshaw, C. M., Berkovitch, S. S., Chang, A., Ham, S., and Verdine, G. L. (2014) Stitched α-helical peptides via bis ring-closing metathesis, *J. Am. Chem. Soc. 136*, 12314-12322.
2. Kim, Y.-W., Grossmann, T. N., and Verdine, G. L. (2011) Synthesis of all-hydrocarbon stapled α-helical peptides by ring-closing olefin metathesis, *Nat. Protoc. 6*, 761-771.

5.2. Figures

V30-SP-1 (>95% purity)

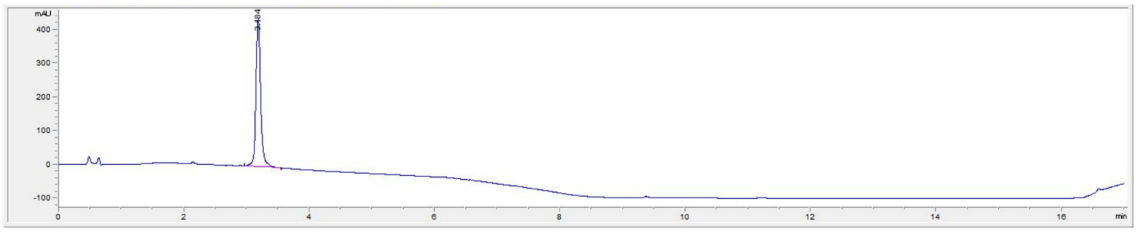

V30-SP-2 (>95% purity)

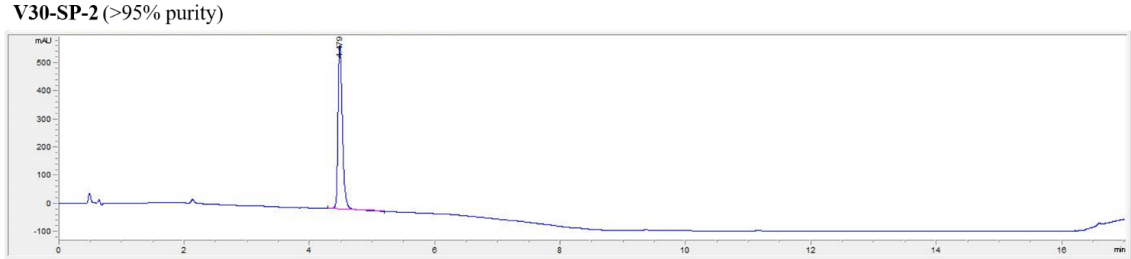

V30-SP-3 (>95% purity)

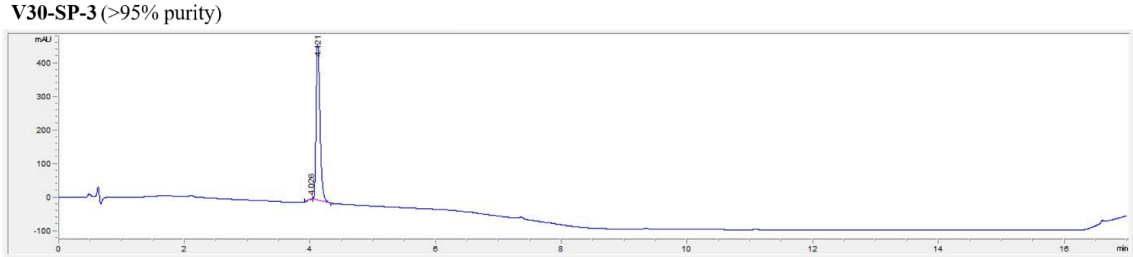

V30-SP-4 (>95% purity)

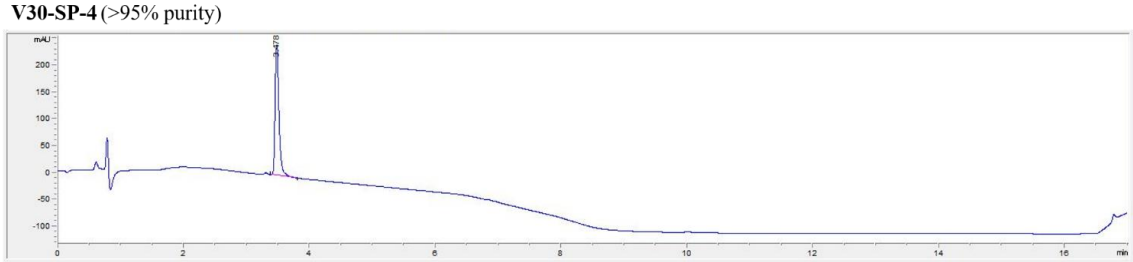

V30-SP-5 (>95% purity)

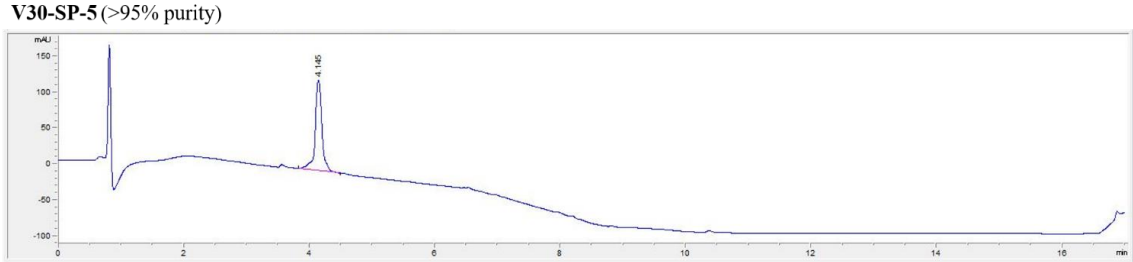

V30-SP-6 (>95% purity)

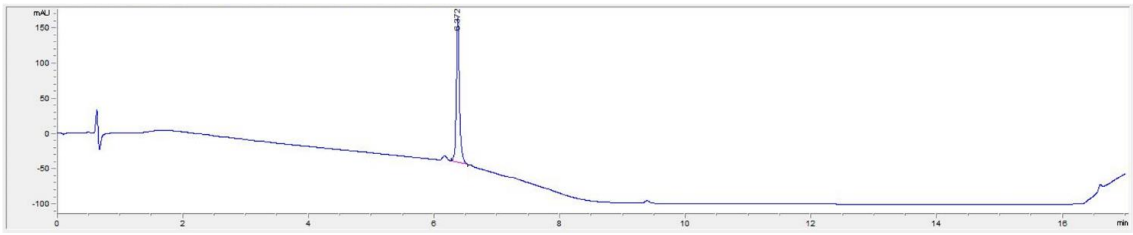

V30-SP-7 (>95% purity)

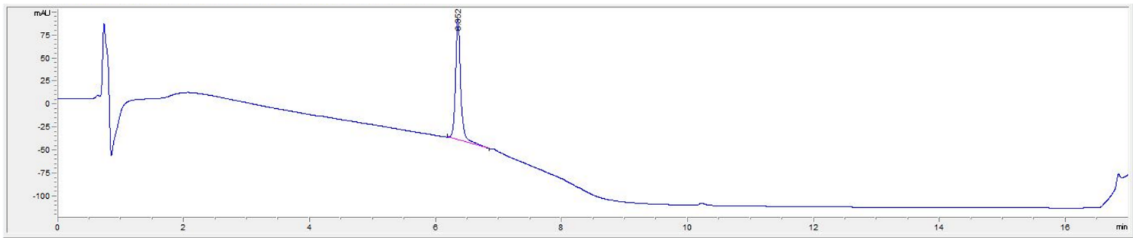

V30-SP-8 (>95% purity)

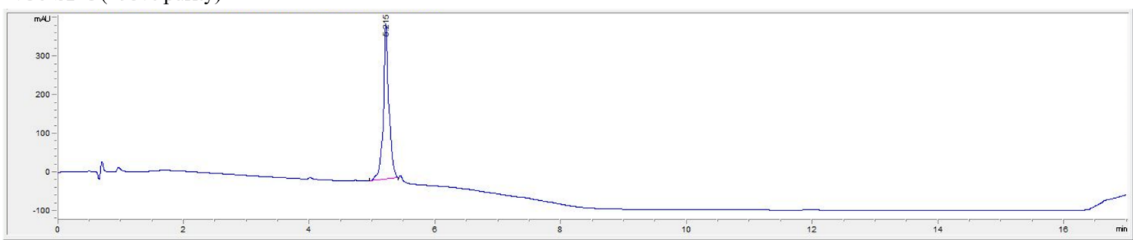

V30-SP-9 (>95% purity)

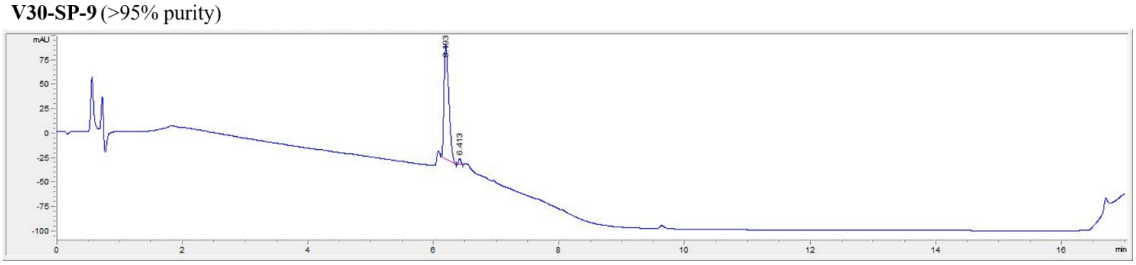

V30-SP-10 (>95% purity)

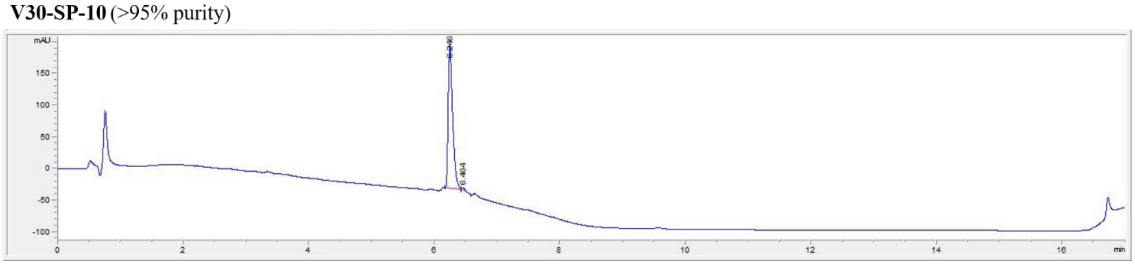

V30-SP-11 (>95% purity)

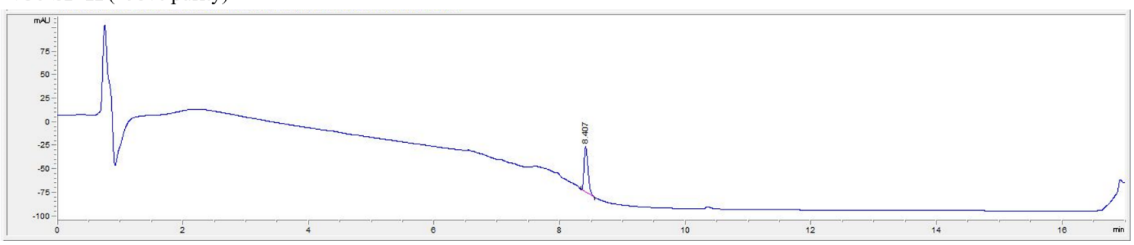

V30-SP-8-FITC (>95% purity)

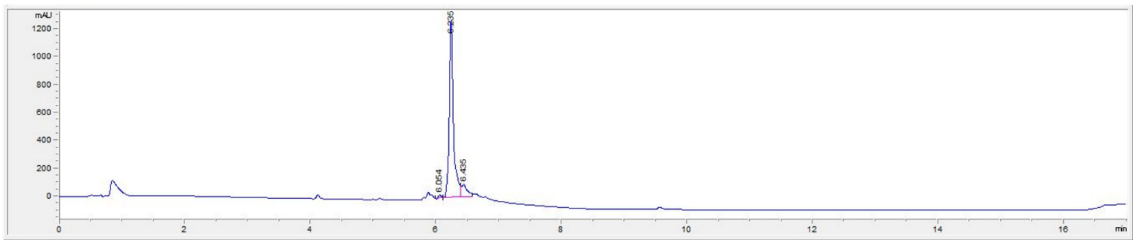

V30-SP-9-FITC (>95% purity)

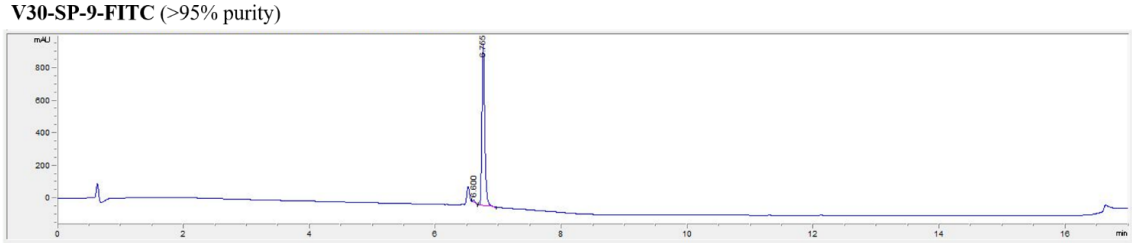

Figure S1. HPLC chromatogram of the purified peptides. All the spectra were measured on an Agilent HP 1260 system (Agilent Technologies, Santa Clara, US). A Zorbax C18 column (2.7 μm, 120 Å, 4.6 × 50 mm) was used for the stationary phase. For the mobile phase, solvent A (water containing 0.1% *v/v* trifluoroacetic acid (TFA)) and solvent B (acetonitrile) were used as a gradient. The gradient was given as follows: i) linear gradient of B from 5 to 50% (0 – 5 min); ii) linear gradient of B from 50 to 100% (5 – 7 min); iii) isocratic hold (B, 100%) (7 – 15 min); and iv) linear gradient of B from 100 to 5% (15 – 17 min). The flow rate was set to 1.0 mL/min.

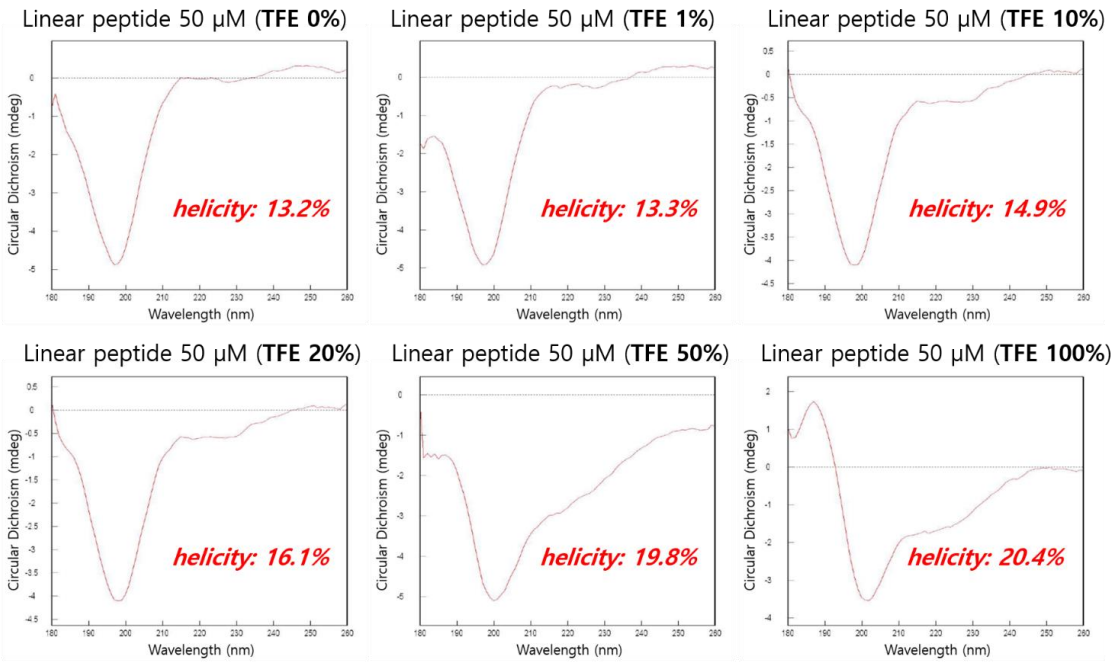

Figure S2. CD spectroscopic analysis of the linear peptide upon the serial increase in TFE.

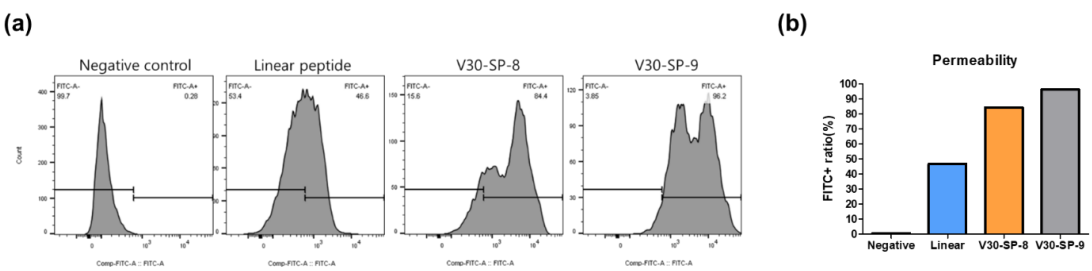

Figure S3. Flow cytometry data. **(a)** Flow cytometry of *M. smegmatis* cells obtained from the untreated (negative control) group and the addition of FITC-labeled peptides (linear form, **V30-SP-8 and V30-SP-9**). **(b)** Bar graph showing the quantitative amount of cellular uptake of each peptide. The activity was normalized to that of **V30-SP-9**.

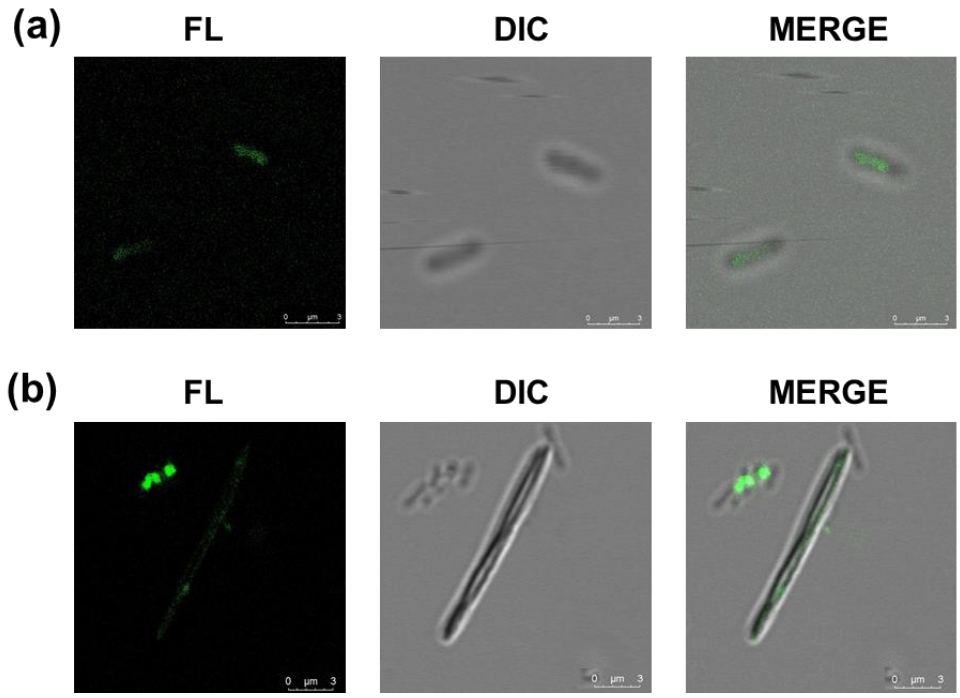

Figure S4. Confocal laser scanning microscopy images of *M. smegmatis* treated with FITC-labeled peptides (10 μM) (left), bright-field images of *M. smegmatis* (middle) and merged images (right). a) V30-SP-8. b) V30-SP-9.

TABLES

Table S1. MS data for the peptides.[a]

Peptide	Sequence	MS(calcd)	MS(obsd)
V30-SP-1	E$\overline{\mathbf{R}_5}$AA$\overline{\mathbf{S}_5}$RHR	1030.59	1030.59
V30-SP-2	E$\overline{\mathbf{S}_5}$AAI$\overline{\mathbf{S}_5}$HR	987.57	987.57
V30-SP-3	ELAA$\overline{\mathbf{R}_5}$RH$\overline{\mathbf{S}_5}$	987.57	987.57
V30-SP-4	R$\overline{\mathbf{R}_5}$GE$\overline{\mathbf{S}_5}$GGRE	1051.56	1051.56
V30-SP-5	R$\overline{\mathbf{R}_8}$GEPGGR$\overline{\mathbf{S}_5}$	1061.62	1061.62
V30-SP-6	AERF$\overline{\mathbf{R}_8}$AAVEAD$\overline{\mathbf{S}_5}$I	1524.84	1524.84
V30-SP-7	DEPDAERF$\overline{\mathbf{R}_8}$AAVEAD$\overline{\mathbf{S}_5}$I	1980.99	1980.99
V30-SP-8	$\overline{\mathbf{S}_5}$LAA$\overline{\mathbf{B}_5}$RH$\overline{\mathbf{S}_5}$	1023.65	1023.65
V30-SP-9	$\overline{\mathbf{R}_8}$LAAIRH$\overline{\mathbf{S}_5}$	1013.66	1013.66
V30-SP-10	R$\overline{\mathbf{R}_5}$GE$\overline{\mathbf{B}_5}$GGR$\overline{\mathbf{R}_5}$	1087.64	1087.64
V30-SP-11	$\overline{\mathbf{R}_8}$PDAERF$\overline{\mathbf{B}_5}$AAVEAD$\overline{\mathbf{S}_8}$	1831.00	1831.00
V30-SP-8-FITC	FITC-Ahx-$\overline{\mathbf{S}_5}$LAA$\overline{\mathbf{B}_5}$RH$\overline{\mathbf{S}_5}$	1483.76	1483.76
V30-SP-9-FITC	FITC-Ahx-$\overline{\mathbf{R}_8}$LAAIRH$\overline{\mathbf{S}_5}$	1473.77	1473.77

[a] All mass spectrometric data correspond to $[M+H]^+$ peaks

Table S2. Primers used in cloning

pYUBDuetVector-Rv0623-Rv0624		
1st PCR	Rv0623-BHI_F	accacagccaggatcc g ATGGCGCTGAGTATCAAG
	Rv0623-Hid_rN	atgcggccgcaagctt TCAGGCCGGCAATCCGCG
2nd PCR	Rv0624-NdeI_F	agaaggagatatacat ATGGTGATCGACACGTCC
	Rv0624-ERV-R	gtggccggccgatatc gc GGGCAGCGCGACCGTGGC

References

1. Kang, S. M., Kim, D. H., Jin, C., and Lee, B. J. (2018) A systematic overview of type II and III toxin–antitoxin systems with a focus on druggability, *Toxins (Basel) 10*, 515.
2. Park, S. J., Son, W. S., and Lee, B. J. (2013) Structural overview of toxin–antitoxin systems in infectious bacteria: a target for developing antimicrobial agents, *Biochim. Biophys. Acta 1834*, 1155–1167.
3. Otsuka, Y. (2016) Prokaryotic toxin–antitoxin systems: novel regulations of the toxins, *Curr. Genet. 62*, 379–382.
4. Slayden, R. A., Dawson, C. C., and Cummings, J. E. (2018) Toxin–antitoxin systems and regulatory mechanisms in *Mycobacterium tuberculosis*, *Pathog. Dis.* 76. doi: 10.1093/femspd/fty039.
5. Yang, Q. E., and Walsh, T. R. (2017) Toxin–antitoxin systems and their role in disseminating and maintaining antimicrobial resistance, *FEMS Microbiol. Rev. 41*, 343–353.
6. Kang, S. M., Kim, D. H., Lee, K. Y., Park, S. J., Yoon, H. J., Lee, S. J., Im, H., and Lee, B. J. (2017) Functional details of the *Mycobacterium tuberculosis* VapBC26 toxin–antitoxin system based on a structural study: insights into unique

binding and antibiotic peptides, *Nucleic Acids Res. 45*, 8564-8580.

7. Williams, J. J., and Hergenrother, P. J. (2012) Artificial activation of toxin-antitoxin systems as an antibacterial strategy, *Trends Microbiol. 20*, 291-298.

8. Lee, I. G., Lee, S. J., Chae, S., Lee, K. Y., Kim, J. H., and Lee, B. J. (2015) Structural and functional studies of the *Mycobacterium tuberculosis* VapBC30 toxin-antitoxin system: implications for the design of novel antimicrobial peptides, *Nucleic Acids Res. 43*, 7624-7637.

9. Schafmeister, C. E., Po, J., and Verdine, G. L. (2000) An all-hydrocarbon cross-linking system for enhancing the helicity and metabolic stability of peptides, *J. Am. Chem. Soc. 122*, 5891-5892.

10. Zaychikova, M. V., Zakharevich, N. V., Sagaidak, M. O., Bogolubova, N. A., Smirnova, T. G., Andreevskaya, S. N., Larionova, E. E., Alekseeva, M. G., Chernousova, L. N., and Danilenko, V. N. (2015) Mycobacterium tuberculosis Type II Toxin-Antitoxin Systems: Genetic Polymorphisms and Functional Properties and the Possibility of Their Use for Genotyping, *PLoS One 10*, e0143682.

11. Billman-Jacobe, H., Haites, R. E., and Coppel, R. L. (1999) Characterization of a *Mycobacterium smegmatis* mutant lacking penicillin binding protein 1, *Antimicrob. Agents Chemother. 43*, 3011-3013.

12. Peteroy, M., Severin, A., Zhao, F., Rosner, D., Lopatin, U., Scherman, H., Belanger, A., Harvey, B., Hatfull, G. F., Brennan, P. J., and Connell, N. D. (2000) Characterization of a *Mycobacterium smegmatis* mutant that is simultaneously resistant to D-cycloserine and vancomycin, *Antimicrob. Agents Chemother. 44*, 1701-1704.

13. Hilinski, G. J., Kim, Y.-W., Hong, J., Kutchukian, P. S., Crenshaw, C. M., Berkovitch, S. S., Chang, A., Ham, S., and Verdine, G. L. (2014) Stitched α-helical peptides via bis ring-closing metathesis, *J. Am. Chem. Soc. 136*, 12314-12322.

14. Kim, Y.-W., Grossmann, T. N., and Verdine, G. L. (2011) Synthesis of all-hydrocarbon stapled α-helical peptides by ring-closing olefin metathesis, *Nat. Protoc. 6*, 761-771.

15. Bohm, G., Muhr, R., and Jaenicke, R. (1992) Quantitative analysis of protein far UV circular dichroism spectra by neural networks, *Protein Eng. 5*, 191-195.

국문초록

독소-항독소 시스템은 박테리아의 생존에 필수적인 요소로 알려져 있습니다. 저희가 결핵균을 타겟으로 하는 신약 개발 과정을 수행하는 동안, 저희 연구실은 VapBC30 복합체의 결합을 모방한 특정 펩타이드들이 박테리아의 성장을 억제하고 결국에는 사멸하게 만든다는 사실을 발견하였습니다. 여기서 저희는 이 후보물질들을 최적화하기 위하여 stapling 기술을 적용한 후, 생물학적 평가를 진행하였습니다. 평가 결과, 여러 후보 물질들 중 V30-SP-8 펩타이드가 *Mycobacterium smegmatis*의 세포벽을 성공적으로 투과하고, 12.5μM과 25.0μM 사이의 농도에서 MIC_{50}를 가진다는 것을 확인하였습니다. *M. tuberculosis*에서 유래한 VapBC30 TA system의 구조 정보와 생화학적인 정보를 바탕으로 잠재적인 새로운 항생물질을 제시하고, 새로운 신약개발의 전략을 제시했습니다. 또한, TA 시스템 기반의 약물은 거의 전무하다는 것을 감안하면, 이것은 단순히 TA 시스템과 연관된 물질을 탐구한 것이 아니라 항결핵제의 새로운 발견을 시작을 시사하는 연구입니다.

주요어 : 독소-항독소, 결핵, 펩타이드, 항생물질, 신약 개발
학 번 : 2019-26322